RSC Advances

PAPER

View Article Online
View Journal | View Issue

Cite this: *RSC Adv.*, 2024, **14**, 7517

3D sponge loaded with cisplatin–CS–calcium alginate MPs utilized as a void-filling prosthesis for the efficient postoperative prevention of tumor recurrence and metastasis

Yihong Yang, Genlan Ye and Xiaozhong Qiu *

Received 3rd November 2023
Accepted 20th February 2024

DOI: 10.1039/d3ra07516h

rsc.li/rsc-advances

Intraoperative bleeding is a pivotal factor in the initiation of early recurrence and tumor metastasis following breast cancer excision. Distinct advantages are conferred upon postoperative breast cancer treatment through the utilization of locally administered implant therapies. This study devised a novel 3D sponge implant containing cisplatin-loaded chitosan–calcium alginate MPs capable of exerting combined chemotherapy and hemostasis effects. This innovative local drug-delivery implant absorbed blood and residual tumor cells post-tumor resection. Furthermore, the cisplatin-loaded chitosan–calcium alginate MPs sustainably targeted and eliminated cancer cells, thereby diminishing the risk of local recurrence and distant metastasis. This hydrogel material can also contribute to breast reconstruction, indicating the potential application of the 3D sponge in drug delivery for breast cancer treatment.

1. Introduction

Breast cancer has emerged as the most frequently diagnosed cancer and is a leading cause of high mortality among women worldwide. This disease accounts for 23% of the total cancer cases and 14% of cancer-related deaths.[1–3] Currently, the common modalities for breast cancer management are surgical resection, radiation therapy, chemotherapy, and targeted therapies.[4,5] Among them, surgical resection remains the cornerstone of early-stage breast cancer treatment and control.[6] However, the incidence of recurrence and metastasis following breast cancer surgery is high, resulting in less-than-ideal long-term prognosis and contributing to elevated postoperative mortality rates.[4] Even in cases of local recurrence, additional surgical interventions are often unfeasible, with tumor recurrence/metastasis accounting for over 90% of all cancer-related deaths.[7,8] Moreover, patient demand is growing for postoperative breast aesthetics.[9–11] Thus, effective strategies for preventing breast cancer recurrence and metastasis, as well as breast reconstruction, play pivotal roles in post-mastectomy survival and recovery.

To mitigate the risk of postoperative recurrence and metastasis, several studies have predominantly focused on radiation therapy, chemotherapy, or targeted treatments. However, these methods exert considerable destructive effects on normal organs and cells, resulting in less-than-ideal treatment outcomes.[12,13] To address these challenges, researchers have proposed strategies involving localized drug-delivery systems, such as drug-loaded microparticles (MPs), gels, films, or fibers.[14–19] On one hand, these approaches enhance the therapeutic efficacy of chemotherapeutic agents. On the other hand, they reduce the toxic side effects.

However, emerging evidence suggests that inevitable intraoperative bleeding, stemming from damage to patients' tissues and vasculature during tumor resection, could lead to the dissemination of tumor cells into the bloodstream.[20] This dissemination elevates the levels of circulating tumor cells (CTCs), thereby heightening the risk of both local recurrence and distant metastasis.[20] Despite the remarkable effects of strategies aimed at minimizing intraoperative bleeding, their full potential in investigating the recurrence and metastasis induced by intraoperative bleeding has not yet been fully recognized. In clinical practice, conventional mechanical and thermal methods are employed to mitigate intraoperative blood loss, but their effectiveness is limited in controlling bleeding from challenging-to-access regions.[21] Accordingly, a localized drug-delivery implant with chemotherapeutic antitumor capabilities and the capacity to absorb postoperative bleeding is needed.

Hydrogels are extensively used in the fields of tissue-engineering repair and drug delivery due to their excellent biocompatibility, porous three-dimensional structure, and straightforward manufacturing techniques.[22–26] Among them, methacrylated gelatin (gel-MA) stands out because of its highly absorbable and hemostatic properties, as well as the methacrylation-generated crosslinking structures that enhance

Guangdong Provincial Key Laboratory of Construction and Detection in Tissue Engineering, School of Basic Medical Science, Southern Medical University, Guangzhou, Guangdong 510515, P. R. China. E-mail: qqiuxzh@163.com

the mechanical strength of the hydrogel.[15,27] This feature makes it particularly well-suited as a drug carrier for facilitating tissue reconstruction and controlling postoperative bleeding.

Cisplatin is the oldest platinum-based anticancer drug in current use despite its well-documented dose-dependent toxicity.[12,28,29] Thus, the targeted delivery of cisplatin to cancer cells is necessary.[30] In the present study, cisplatin–chitosan (CS)–calcium alginate MPs were constructed. Cisplatin was encapsulated within the MPs through crosslinking interactions with the positively charged polymer CS and the negatively charged polymer sodium alginate. This encapsulation method effectively reduced the rate of cisplatin release from the MPs. The crosslinking reaction between alginate, CS, and the respective crosslinkers is illustrated in Fig. 1.

We used ion crosslinking gelation technology to prepare a cryogel composite sustained-release system loaded with cisplatin–CS–calcium alginate MPs. This system, upon contact with blood, exhibited sponge-like characteristics, absorbing and expanding upon blood contact. It also possessed adhesive properties, enabling it to adhere onto bleeding sites, absorb blood, and induce platelet aggregation for clot formation. Simultaneously, circulating tumor cells dispersed in the blood accumulate within this sponge. Through interactions with cisplatin–loaded CS–calcium alginate MPs, the MPs released cisplatin to effectively target and eliminate residual cancer cells within the sponge and the circulating tumor cells present in the bloodstream. Therefore, this approach reduced the risk of tumor recurrence and metastasis.

Additionally, the MPs were loaded into the gel-MA help increase the strength of gel-MA and realize a long-term *in situ* function. We examined the characteristics and performance of the constructed composite sustained-release system, its impact on the proliferation and apoptosis of MDA-MB-231-luc cells *in vitro* and *in vivo*, and the *in vitro* coagulation and *in vivo* hemostasis abilities of the composite sustained-release system. The effectiveness of the composite sustained-release system in preventing postoperative tumor recurrence and metastasis was further explored in an animal model. The 3D sponge loaded with cisplatin–CS–calcium alginate MPs was utilized as a promising void-filling prosthesis for the efficient post-operative prevention of tumor recurrence and metastasis.

2. Materials and methods

2.1. Reagents and materials

Cisplatin was purchased from Meryer (Shanghai) Chemical Technology Co., Ltd. CS and sodium alginate were purchased from Shanghai Macklin Inc. $CaCl_2$ was purchased from Sun

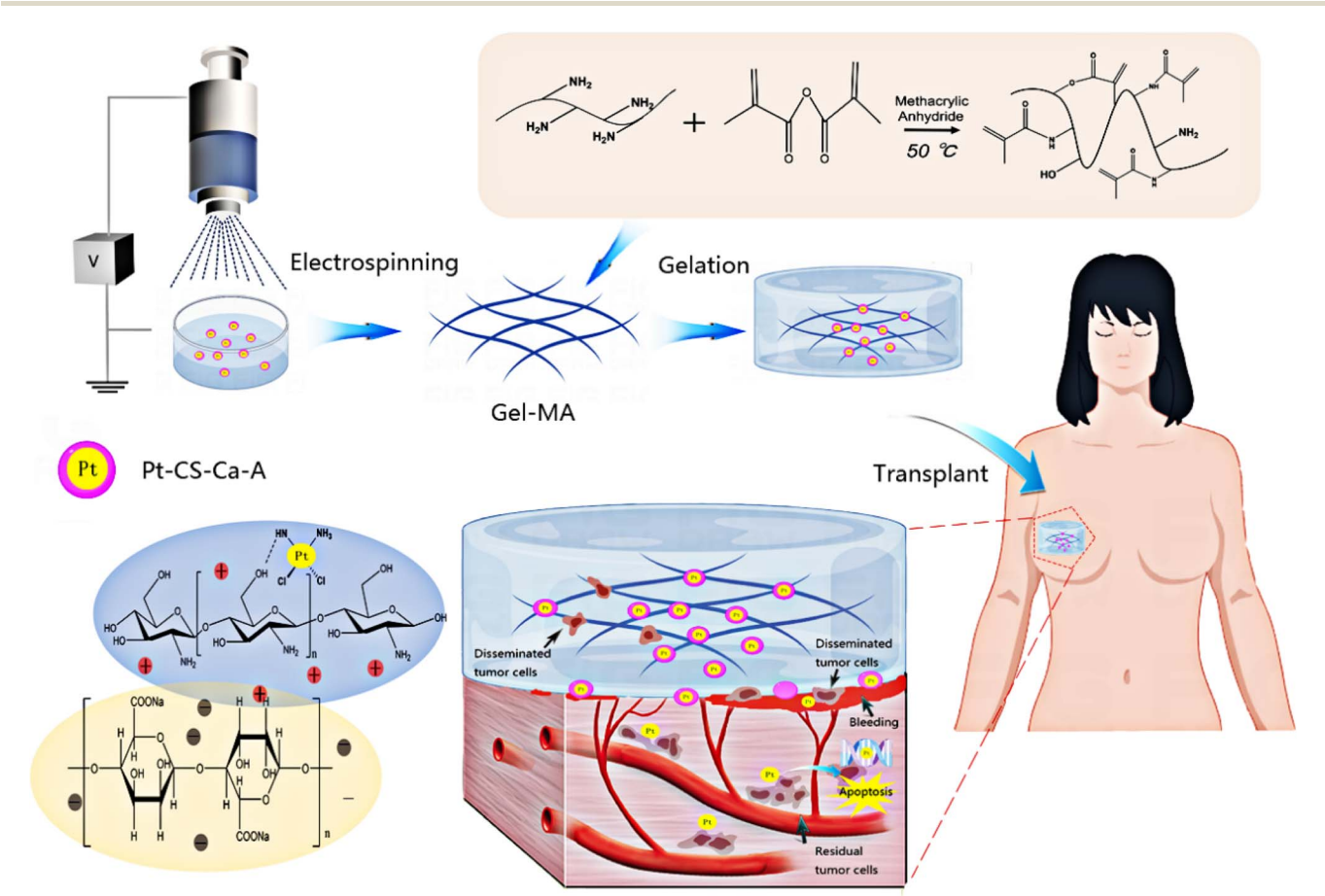

Fig. 1 Illustration of 3D sponge loaded with cisplatin–CS–calcium alginate MPs combining chemotherapy and hemostasis for the efficient postoperative prevention of tumor recurrence and metastasis.

Chemical Technology (Shanghai) Co., Ltd. Gelatin was purchased from Shanghai Haohong Scientific Co., Ltd. Methacrylic anhydride, glacial acetic acid, and tetramethylenediamine were purchased from Meryer (Shanghai) Chemical Technology Co., Ltd. APS was purchased from Guangzhou Chemical Reagent Factory. Phosphate buffer and Duchenne phosphate buffer were purchased from Beijing Solarbio Science & Technology Co., Ltd. PEGDA was purchased from Shanghai Aladdin Biochemical Technology Co., Ltd. Rabbit anti-γH2AX antibody was purchased from Abcam Plc. 4′,6-Diamidino-2-phenylindole was bought from Sigma. Horseradish peroxidase-labeled goat anti-rabbit IgG antibody and Live & Dead Viability/Cytotoxicity Assay Kit was bought from Invitrogen Trading (Shanghai) Co., Ltd. Cell-CountingCCK-8 was bought from Dojindo Molecular Technologies (Japan). TUNEL apoptosis detection kit was bought from Promega (Beijing) Biotech Co., Ltd. Dulbecco's modified Eagle medium (DMEM), fetal bovine serum, and penicillin–streptomycin mix were purchased from Thermo Fisher Scientific Inc. All the other reagents and materials were used as received.

2.2. Preparation and characterization of cisplatin–CS–calcium alginate MPs

Cisplatin–CS–calcium alginate MPs were prepared by electrospinning. Initially, a solution was prepared by mixing 5 mL of 2 mM cisplatin and 5 mL of 1% CS, and this mixture was allowed to stand overnight. This solution was then combined with a 1% sodium alginate solution and thoroughly stirred to create a homogenous mixed solution.

For electrospinning, the mixed solution from the previous step was loaded into a plastic syringe equipped with a 21 G metal spinneret. The syringe was connected to a high-voltage power supply (Beijing Vealery Technology Development Company) with an applied voltage of 15 kV. The distance between the needle and the collector was maintained at 16 cm, and the flow rate was set to 2 mL h^{-1}. The collector comprised a 10% calcium chloride solution.

The resulting MPs were then subjected to a series of post-processing steps. First, they were washed three times with deionized water and subsequently centrifuged at 900 rpm min^{-1} for 5 min. After centrifugation, the MPs were freeze dried for a period of 2 days in a freeze-drying machine and then stored in a desiccator for use in subsequent experiments.

To evaluate their physical characteristics, the appearance of the MPs was examined using a standard optical microscope and a scanning electron microscope.

2.3. Preparation and characterization of hydrogel 3D sponge

Cryogels containing varying concentrations (6, 12, 18, and 24 mg) of MPs were synthesized through ion crosslinking. The MPs were dispersed in 100 μL of a 10% gel-MA distilled water solution. Subsequently, 100 μL of 8.33% PEGDA was added to the mixture, followed by the addition of 400 μL of distilled water. To initiate the catalytic reaction, 9 μL of 20% APS and 3 μL of tetramethylethylenediamine were added to the mixture, ensuring immediate and thorough mixing. The resulting mixture was then poured into molds and placed in a refrigerator at −20 °C overnight to induce gelation, forming the frozen hydrogel.

The formation of hydrogen bonds within the cryogel was analyzed by nuclear NMR. ATR-FTIR spectroscopy (Thermo Scientific IR6700) was used to investigate the chemical bonds present within the cryogel. The surface structure and the distribution of internal MPs within the cryogel were visualized using a field-emission scanning electron microscope.

To conduct mechanical testing, the cryogels containing varying concentrations of cisplatin–CS–calcium alginate MPs were uniformly cut into rectangular samples measuring 5 cm × 1 cm. Stress–strain experiments were conducted on each sample, with each test being repeated three times, by using a Universal Testing Machine at a constant speed of 50 mm min^{-1} to generate stress–strain curves.

2.4. *In vitro* hemostasis capability

To assess the extent of lyophilized hydrogel swelling, the hydrogel samples were immersed in a predetermined volume of PBS at 37 °C. At specified intervals, the swollen hydrogel was weighed after gently blotting away excess water with tissue paper. The experiment continued until no further change in the swelling ratio was observed. The swelling percentage was calculated using the following equation: degree of swelling (%) = $(W_s - W_d/W_d) \times 100$, where W_s and W_d represent the weights of the hydrogel sample in the swollen and lyophilized states, respectively. Quantitative values are presented as means ± standard deviation, with a sample size of $n = 3$.

Mouse-blood sample collection was retro-orbital blood collection. The absorbance of distilled water (50 mL) and whole blood (100 μL) solutions at 540 nm was set to 100 as a reference value. The BCI of different materials was calculated as follows: BCI = blood absorption in contact with the material at 540 nm/whole blood absorption in water at 540 nm. The material was placed in a beaker, and 100 μL of whole blood droplets containing EDTAK2 was added onto the surface of the material. After incubation at 37 °C for 5 min, 50 mL of distilled water was added slowly. For the control group, we placed 100 μL of whole blood droplets on a culture dish. The coagulation index was measured using a microplate reader (Thermo Scientific).

2.5. *In vitro* cytotoxicity of hydrogel assay

The *in vitro* cytotoxicity assessment of cryogel and cryogel composite MPs with varying concentrations toward MDA-MB-231-luc cells was conducted by the CCK-8 assay.

MDA-MB-231-luc was purchased from Shanghai Zhongqiao Xinzhou Biological Technology Co., Ltd. MDA-MB-231-luc was added to high-glucose DMEM with 10% fetal bovine serum (GIBCO), 100 U mL^{-1} penicillin, and 100 μg mL^{-1} streptomycin. The cells were cultivated separately in a 37 °C, 5% CO_2 incubator, with the culture medium replaced every 2 days.

To initiate the assay, a cell suspension was prepared at a concentration of 10 000 cells per well and subsequently seeded onto 96-well plates. These plates were then incubated at 37 °C for 24 h to allow the cells to adhere and establish. The respective

cryogel and cryogel composite MPs were then introduced into the wells, and the cells were subjected to an additional 24 h incubation.

In the final step of the assay, the CCK-8 stock solution was diluted at a 1 : 9 ratio using the basic culture medium DMEM. Subsequently, 100 μL of this diluted culture medium was added to each well, and the cells were incubated for an additional 1 h. The absorbance of the samples was measured at 450 nm by using a microplate reader (Thermo Scientific).

2.6. *In vivo* hemostatic capability assay

Nude mice (female, 4–6 weeks) and BALB/c mice (female, 6–8 weeks) were purchased from the animal experimental center of Southern Medical University. All animals were housed under pathogen-free conditions in 12 h light–dark cycles with relative humidity of 50–60% and constant room temperature (20 ± 1 °C). All mice were adapted for 7 days before treatment.

By exposing the liver on the left abdominal wall of anesthetized mice, a transverse incision was made on the liver until bleeding occurred. Different materials were placed on the bleeding liver and pressed for 5 min. The BALB/c mice were randomly divided into three groups with specific treatments. (1) The control group received no treatment. (2) Cryogel was placed on the bleeding liver and held in position for 5 min. (3) Cryogel-M-1, of equivalent dimensions, was applied to the bleeding liver and pressed for 5 min. (4) Cryogel-M-2, also of comparable dimensions, was placed on the bleeding liver and compressed for 5 min. (5) Cryogel-M-3, with the same size as the previous samples, was positioned on the bleeding liver and compressed for 5 min. (6) Cryogel-M-4, identical in size to the other materials, was situated on the bleeding liver and compressed for 5 min.

The assessment of hemostatic efficacy involved the direct observation and recording of liver bleeding in mice subjected to gelatin sponge and various other materials. Additionally, the survival rates of mice treated with different materials were evaluated on day 7.

2.7. Immunofluorescence assay

The expression of γ-H2AX was measured when MDA-MB-231-luc was co-cultured with different composite materials for 24 h. The sample slices was fixed with 4% paraformaldehyde at room temperature for 20 min. Slices with antibody γ-H2AX (1 : 800 diluted in 2% BSA) were placed in a wet box at 37 °C for 1 h and then placed in darkness with the secondary antibody in 2% BSA at 37 °C for 1 h. The sample was observed under an inverted laser confocal microscope (CLSM) system. The percentage of fluorescence in the image from three different positions was measured, and the images of each sample were obtained using Image-J software.

2.8. Establishment of breast cancer recurrence model and efficacy evaluation

To assess the anti-recurrence and anti-metastasis effects of various materials in mice, we established a subcutaneous breast cancer recurrence and metastasis model in nude mice. MDA-MB-231-luc cells were subcutaneously injected at a concentration of 5×10^6 cells per 100 μL of PBS. The mice were randomly divided into three groups ($n = 5$). When the mouse's tumor volume reached approximately 100 mm^3, 90% of the tumor was surgically removed, leaving the remaining 10%, and then the following materials were implanted: (1) cryogel, (2) cryogel-M-1, (3) cryogel-M-2, (4) cryogel-M-3, and (5) cryogel-M-4. After a period of 30 days, all mice were euthanized.

The tumors removed from recurrent mice were fixed in a 4% paraformaldehyde solution and embed in paraffin. The thickness of the tumor and organ embedded in paraffin was 2 μm. Slices with antibody γ-H2AX (1 : 800 diluted in 2% BSA and PBS) were placed in a wet box at 37 °C for 1 h and then placed in darkness with the secondary antibody in 2% BSA at 37 °C for 1 h. The tissue slices were used for *in situ* nick-end labeling to detect nuclear DNA fragments with TUNEL cell apoptosis. The sample was observed in an inverted CLSM system. The percentage of fluorescence in the image from three different positions was measured, and the images of each sample were obtained using Image-J software.

2.9. Statistical analysis

Statistical analysis was performed by one-way ANOVA for multiple-group comparisons using SPSS 20.0 software (Chicago, IL, USA). Data are expressed as the mean ± standard deviation, wherein significance was indicated by P value. $P < 0.05$ (*), $P < 0.01$ (**), $P < 0.001$ (***). $P < 0.05$ was considered to indicate statistical significance.

3. Results and discussion

3.1. Characterization of hydrogel loaded with cisplatin–CS–calcium alginate MPs

Two main methods are used to load drugs into a drug carrier. In the first one, monomers are mixed with the drug, initiator and crosslinker followed by polymerization, which trapped the drug within the matrix.[31,32] In the second method, MPs are allowed to swell in a known concentration of drug solution. The drug-loaded MPs are dried to obtain the device. In this work, the former method was used. Under the influence of a high-voltage electrostatic field, the cisplatin–CS–sodium alginate solution was atomized into droplets through a stainless-steel nozzle, which was then deposited into a stirring receiving solution. This step led to the formation of cisplatin–CS–calcium alginate MPs.

The bright-field image of MPs in solution is depicted in Fig. 2A and B, revealing predominantly spherical particles within a size range of 150–350 μm. The average particle size measures 248 μm, and due to the expansive effects in the solution, the particle size distribution exhibits a broader width and non-uniform shape. The particle size distribution of MPs after freeze-drying was characterized using scanning electron microscopy (SEM), as illustrated in Fig. 2C–G. The particles exhibit near-spherical shapes with a smooth and uniform surface, featuring minor protrusions. The particle size range falls within 100–180 μm, with an average size of 132 μm. As depicted in Fig. 2H, in comparison to MPs in solution, the

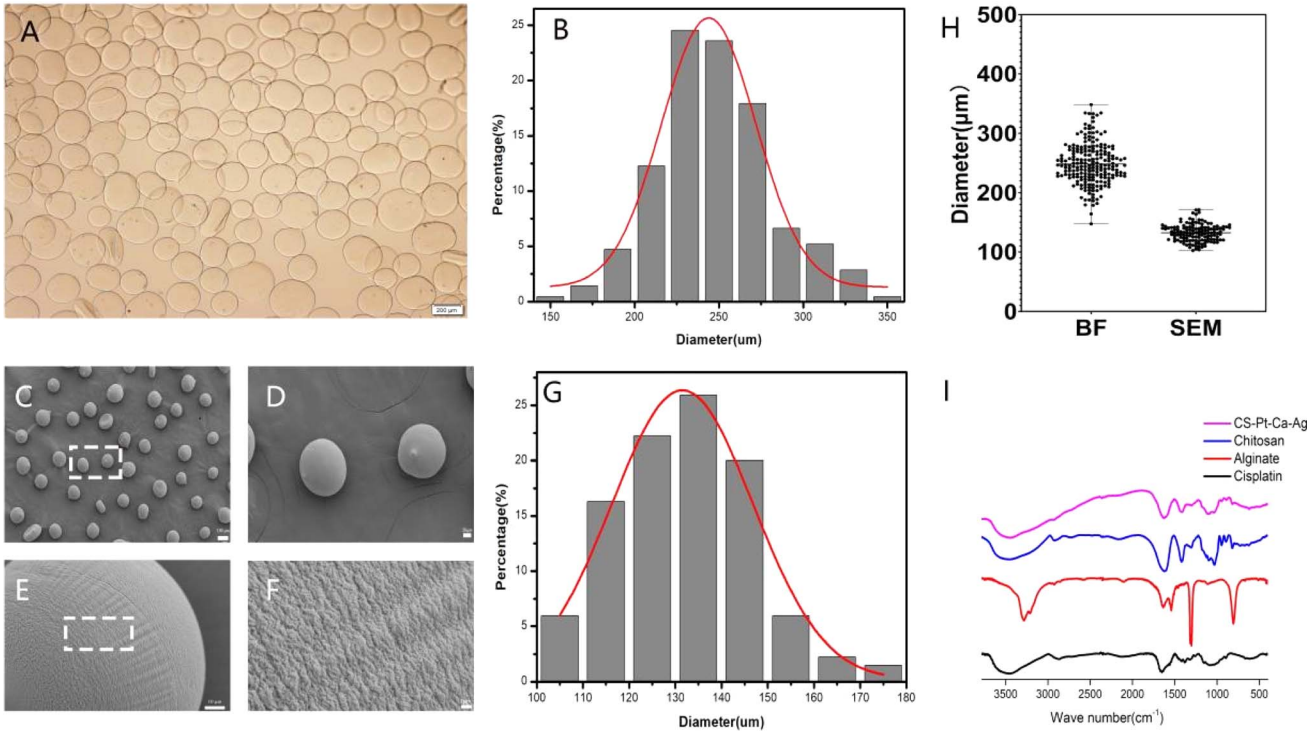

Fig. 2 Characterization of cisplatin–CS–calcium alginate MPs. (A) Bright-field (BF) view of cisplatin–CS–calcium alginate MPs. Scale bar = 200 μm. (B) Size of cisplatin–CS–calcium alginate MPs in bright-field view. (C) Representative SEM images of cisplatin–CS–calcium alginate MPs. Scale bar = 100 μm. (D) Magnified portion of (C). Scale bar = 20 μm. (E) Magnified portion of (D). Scale bar = 10 μm. (F) Magnified portion of (E). Scale bar = 1 μm. (G) Size of cisplatin–CS–calcium alginate MPs in SEM view. (H) Diameter distribution of cisplatin–CS–calcium alginate MPs. (I) FT-IR spectra of the cisplatin, alginate, CS, and CS–Pt–Ca–Ag composite MPs.

freeze-dried particles demonstrate a relatively uniform particle size distribution. The cumulative distribution analysis indicates that 90.37% of particles have sizes below 145 μm. These observations underscore the consistency in the particle size characteristics of MPs, particularly after the freeze-drying process.

Fourier transform infrared (FTIR) spectroscopy was adopted to characterize the existing potential interactions in the MPs. The observed spectra of cisplatin, alginate, CS, and cisplatin–CS–calcium alginate MPs are shown in Fig. 2I. The peak of the stretching vibration of the N–H bond of cisplatin was at 3500 cm^{-1}. The wave peaks of sodium alginate near 3300–3500 and 1720 cm^{-1} indicated that the system contained numerous –OH, –NH, and C=O groups. These characteristic absorption peaks suggested the presence of sodium alginate. CS also contains a large amount of –OH, –NH, and C=O groups, characteristic absorption peaks were found at around 3300–3500 and 1720 cm^{-1}. Finally cisplatin–CS–calcium alginate MPs showed an enhanced peak area due to the characteristic peaks of cisplatin, CS, and sodium alginate at 3300–3500 cm^{-1}. These results indicated that the carboxylic groups of alginate were associated with the ammonium groups of CS through electrostatic interactions to form the polyelectrolyte complex.

Researchers have reported the successful synthesis of gel-MA.[15,33] Gel-MA has many large pore structures, as indicated in Fig. 3A and B. The pore size of gel-MA was determined using ImageJ software, revealing an average diameter of 38.86 ± 8.92 μm for its porous structure. The size of hydrogel pores directly affected the blood absorption capacity, and a porous structure in the hydrogel was more conducive to cell proliferation and differentiation. The ^1H nuclear magnetic resonance (NMR) spectrum of gel-MA indicated that the methacryloyl modification of gelatin was achieved, as shown in Fig. 3C. The peaks at 5.4 and 5.6 ppm were due to the hydrogen of the methacrylic acid double bond, and the peaks at approximately 1.87 ppm were related to the methacrylic acid group of methacrylic acid. These results proved that we successfully synthesized gel-MA.

The MPs were then catalyzed with methacrylic anhydride gelatin (gel-MA) through poly(ethylene glycol) diacrylate (PEGDA) and ammonium persulfate (APS) at low temperature (−20 °C) to form a cryogel composite material loaded with cisplatin–CS–calcium alginate MPs. To further investigate the influence of adding cisplatin–CS–calcium alginate MPs on the structure and antitumor effects of the gel composite material, we prepared gel composites loaded with MPs at different concentrations. The samples were denoted as cryogel-M-1 (10 mg mL^{-1}), cryogel-M-2 (20 mg mL^{-1}), cryogel-M-3 (30 mg mL^{-1}), and cryogel-M-4(40 mg mL^{-1}). As shown in Fig. 3D, according to the SEM image of the loaded cisplatin–CS–calcium alginate MP hydrogel composite, the cisplatin–CS–calcium alginate MPs of cryogel-M-1 group were more dispersed in the cryogel, and the particle size was consistent with the particle size measured before the cryogel was added. The greater the quantity of cisplatin–CS–calcium alginate MPs added, the more

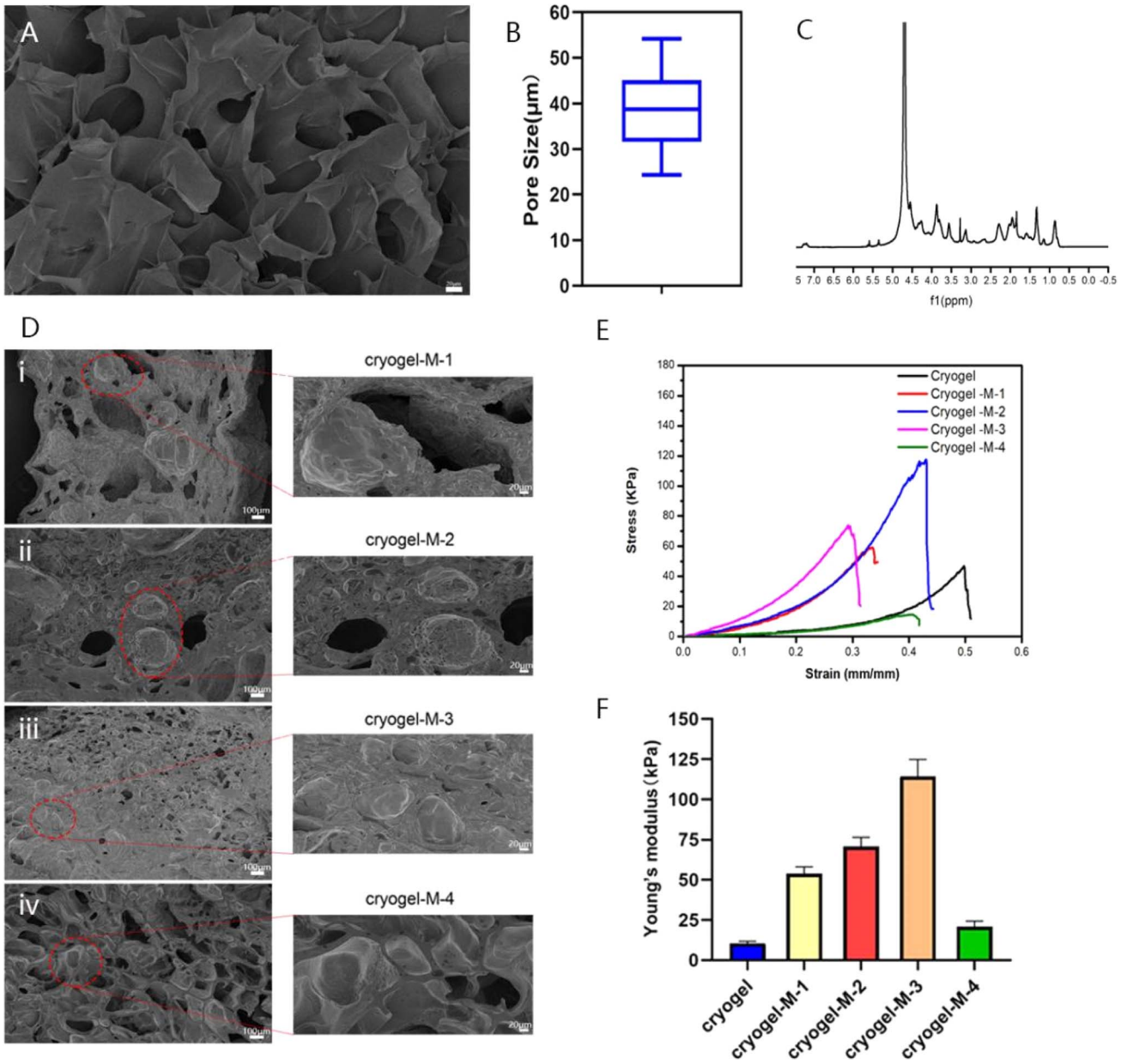

Fig. 3 Characterization of gel-MA. (A) SEM image of gel-MA. Scale bar = 20 μm. (B) Pore size of gel-MA. (C) ^{1}H NMR spectra of gel-MA. The peaks at 5.4 and 5.6 ppm were assigned to two H methacrylic double bonds, and the peak around 1.87 ppm was related to the methacrylate groups of methacrylic acid. (D) Characterization of hydrogel loaded with cisplatin–CS–calcium alginate MPs. (i–iv) SEM images of 3D sponge loaded with cisplatin–CS–calcium alginate MPs and partial magnified SEM images of 3D sponge loaded with cisplatin–CS–calcium alginate MPs. (E) Stress–strain curves of the different materials. (F) Young's modulus of different materials (n = 3).

MPs were present in the gel composite material. Furthermore, the microstructure retained a significant number of porous structures without adversely affecting the blood-absorption capability of the composite material.

To verify the difference in mechanical properties between our synthesized 3D cryogel and those of human breast tissue, compression experiments were performed to test the stress–strain curves of different materials, characterizing the Young's modulus and elasticity of the frozen adhesive. As displayed in Fig. 3E and F, the stress–strain data showed that the elastic coefficients of the frozen adhesive, cryogel-M-1, cryogel-M-2, cryogel-M-3, and cryogel-M-4 were 10.55 ± 1.25, 53.89 ± 4.26, 70.67 ± 5.78, 114.29 ± 10.59, and 20.92 ± 3.47 kPa, respectively. With increased MP amount, the strength of the composite gel system initially increased and then decreased. The main principle behind this phenomenon was that the MPs can initially form crosslinking interactions with the gel. However, increased quantity disrupted these crosslinking interactions, leading to reduced strength. Thus, the addition of MPs to a certain extent affected the mechanical properties of the cryogel. Previous studies have shown that human breast tissue has a certain degree of elasticity. After verification, the mechanical properties of

cryogel + M-4 were closer to those of human breast tissue.[34] These results indicated that our synthesized 3D cryogel loaded with cisplatin–CS–calcium alginate MPs can achieve filling effects *in vivo*, especially after surgery. Thus, it can be expected to replace human breast tissue. Moreover, MPs can help increase the gel strength to realize a long-term *in situ* function *in vivo*.

3.2. *In vitro* and vivo hemostatic capability

The 3D cryogel we synthesized had a dual mechanism for promoting blood clotting. On one hand, its porous structure enabled the absorption of blood, facilitating platelet aggregation to achieve hemostasis.

We characterized the absorption capacity of the 3D cryogel through a swelling experiment, and the results are depicted in Fig. 4B. The swelling percentages were as follows: freeze-dried gel, 9.39 ± 1.37%; cryogel-M-1, 10.36 ± 1.40%; cryogel-M-2, 9.24 ± 2.61%; cryogel-M-3, 12.83 ± 0.33%; and cryogel-M-4, 9.61 ± 2.59%. These values represent the extent of expansion, indicating the ability of the cryogel to absorb blood.

The coagulation effect of the different materials and medical gelatin sponge on blood in water was studied, as shown in Fig. 4A. An equal amount of whole blood was set as the control group, with a blood coagulation index (BCI) of 100%. The BCI is shown in Fig. 4C. The average BCIs were as follows: gelatin sponge, 56.71 ± 5.81%; freeze-dried gel, 57 ± 5.82%; cryogel-M-1, 56.38 ± 5.5%; cryogel-M-2, 47.05 ± 6.22%; cryogel-M-3, 46.41 ± 4.72%; and cryogel-M-4, 46.45 ± 4.74%. The BCIs of cryogel-M-2 and cryogel-M-1 were equivalent to that of the market gelatin sponge and lower than that of the whole blood control group. The BCIs of cryogel-M-3 and cryogel-M-4 were lower than those of the market sponge, cryogel-M-2, and cryogel-M-1. The lower the BCI, the better the coagulation effect, indicating that the freeze-dried gel loaded with cisplatin–CS–calcium alginate MPs can achieve rapid coagulation *in vitro*.

Gelatin and CS, as integral components of the composite, offer exceptional hemostatic properties and promote wound healing.[35] As shown in Fig. 4D, the composite's capacity for hemocyte adsorption and platelet activation enabled it to demonstrate outstanding hemostatic efficacy in a liver injury model. Control mice had a 7 days postoperative survival rate of only 60%, whereas the group treated with freeze-dried hemostatic gel loaded with cisplatin–CS–calcium alginate MPs achieved a 7 days survival rate of 100%. It is noteworthy that all mice in the experimental group survived, presenting a stark contrast to the control group. *In vivo* hemostasis experiments conclusively demonstrated the excellent hemostatic effects of the freeze-dried gel incorporated with composite MPs, highlighting its promising application prospects.

3.3. *In vitro* cell viability experiments

To assess the anticancer efficacy of the hydrogel platform on breast cancer cell viability, cell activity was evaluated with a Cell-Counting Kit-8 (CCK-8).

Fig. 4E shows that after co-culture with breast cancer cells, cryogel-M-1, cryogel-M-2, cryogel-M-3, and cryogel-M-4 loaded with different cisplatin–CS–calcium alginate MPs were set as the control group. The activity percentages of cryogel-M-1, cryogel-M-2, cryogel-M-3, and cryogel-M-4 were 49.43 ± 1.96%, 39.85 ± 6.37%, 33.05 ± 12.78%, and 24.78 ± 3.84%, respectively. As the concentration of MPs in the cryogel increased, the composite material loaded with cisplatin–CS–calcium alginate MPs had greater toxicity to cells. *In vitro* cell viability test showed that the composite materials loaded with different cisplatin–CS–calcium alginate MPs better inhibited the proliferation of breast cancer cells. This finding was attributed to the successful encapsulation of cisplatin drugs within the MPs, which subsequently led to a gradual release of the drug during co-cultivation with breast cancer cells, resulting in the death of a portion of the breast cancer cells. In this study, a well-established drug-loaded microsphere system was employed, the sustained-release efficacy of which has been validated in numerous research investigations. Harpal *et al.* utilized ionotropic gelation techniques to fabricate cisplatin-loaded chitosan-coated spray-dried particles.[36] In comparison to ordinary drug particles, uncoated, and coated particles, cisplatin exhibited an extended release duration by 24 hours. Motasem *et al.* assessed microspherical particles based on alginate–chitosan without conventional cross-linking agents for the targeted delivery of cisplatin through intratracheal administration.[37] The continuous release of cisplatin surpassed 6 hours in this particular context. Therefore, based on this system the MPs can play a role in padding the breast, and their degradation and slow metabolism can help in breast reconstruction.

Cisplatin exerts its inhibitory effect on cell proliferation by interacting with DNA.[38–40] To investigate the mechanism of action of this composite material on tumor cells, MDA-MB-231-luc cells cultured in the presence of these materials were subjected to immunofluorescence assay. γ-H2AX serves as a vital marker for DNA breaks.[28] DNA double-strand breaks trigger the phosphorylation of H2AX at the serine 139 position, forming γ-H2AX.[41] Histone H2AX plays a crucial role in DNA damage repair, regulation of cell-cycle checkpoints, maintenance of genomic stability, and tumor suppression.[42]

As illustrated in Fig. 4F, the green fluorescence represents γ-H2AX protein, and the blue fluorescence represents the nucleus. The cryogel group exhibited no γ-H2AX expression, whereas cryogel-M-1, cryogel-M-2, cryogel-M-3, and cryogel-M-4 showed γ-H2AX expression. It is noteworthy that the fluorescence intensity of γ-H2AX immunofluorescence images was quantified using ImageJ, as shown in Fig. 4G. With the increasing concentration of MPs in the cryogel, the expression of γ-H2AX also increased. The cryogel-M-4 group exhibited the highest fluorescence intensity of γ-H2AX expression, indicating that these composites disrupted DNA within cells, leading to the formation of γ-H2AX.

This finding further confirmed that these composites released cisplatin into cells, where the released cisplatin bound to cellular DNA, resulting in DNA double-strand breaks.

3.4. *In vivo* antitumor effect experiment

The antitumor efficiency of the hydrogel platform against breast cancer was further investigated *in vivo*. In clinical practice,

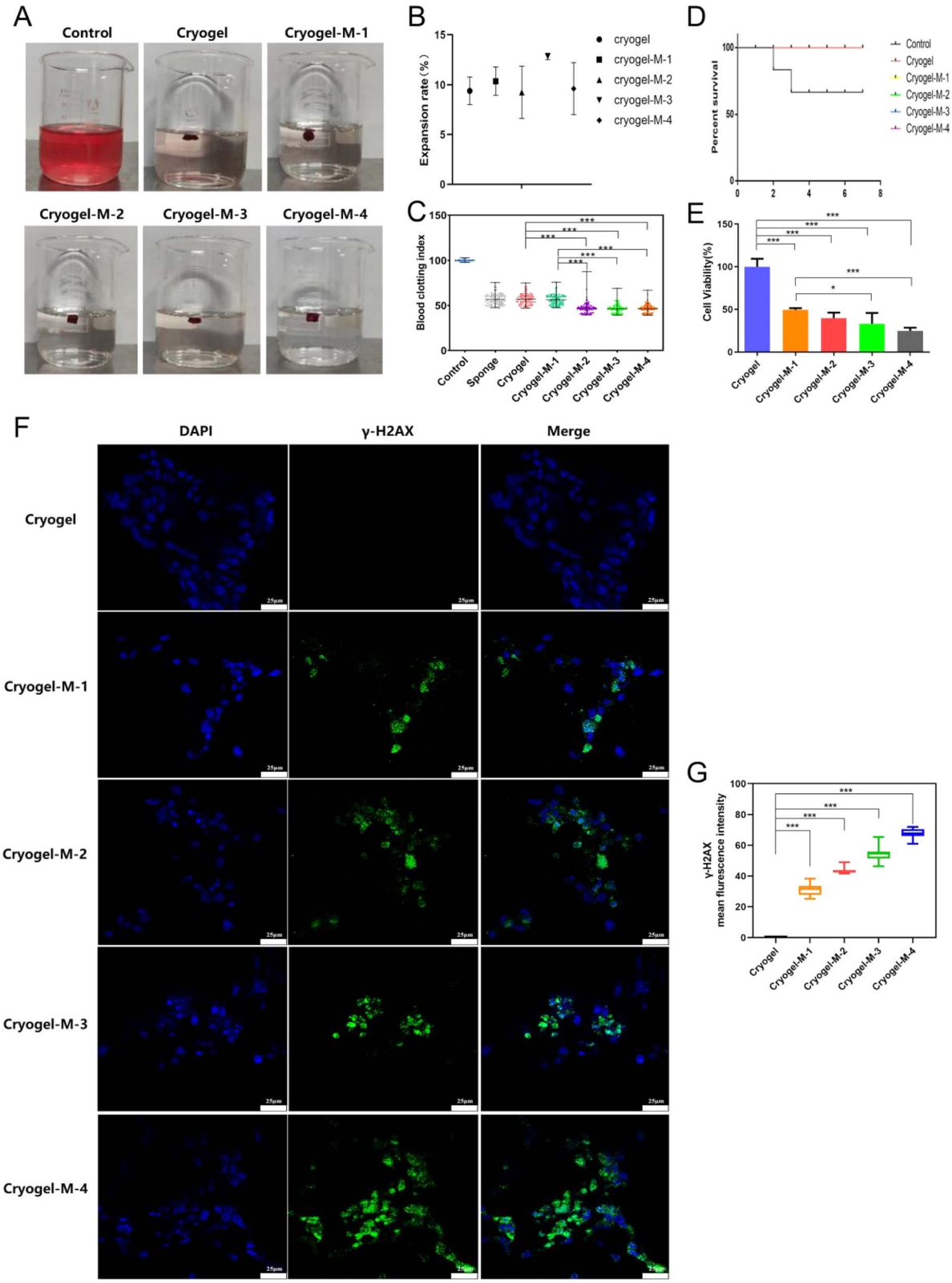

Fig. 4 (A) Photographs taken during blood clotting. (B) Swelling rate of different materials ($n = 3$). (C) The corresponding blood clotting index of different materials. (D) Seven-days survival rate of mice after treatment ($n = 5$). (E) Cell-viability curves of cancer cells after the incubation of different drugs for 24 h. (F) Immunofluorescence image of γ-H2AX in MDA-MB-231-luc cells after coculturing with different materials. Scale bar = 25 μm. (G) Mean fluorescence intensity of γ-H2AX in MDA-MB-231-luc cells after coculturing with different materials ($n = 3$).

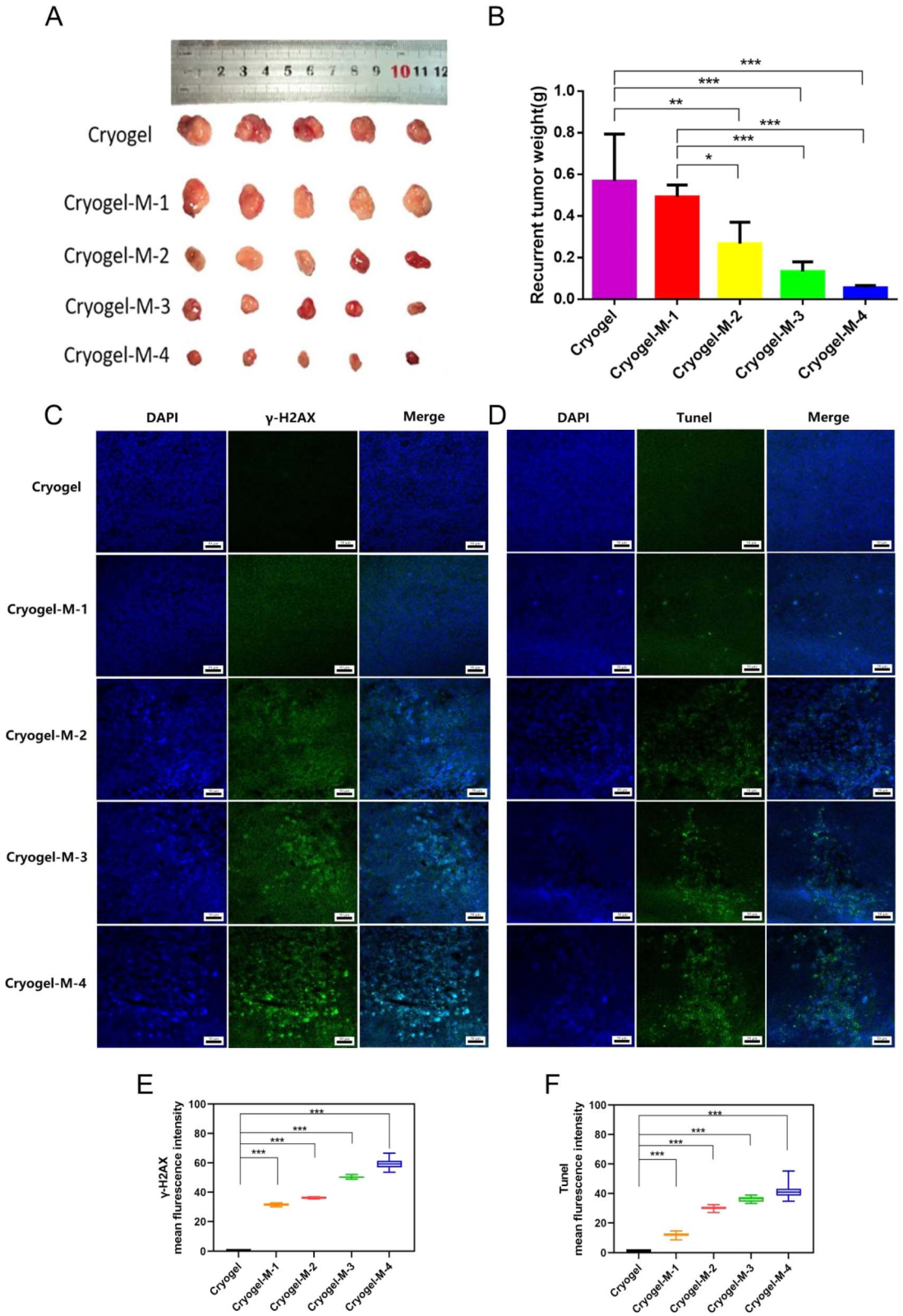

Fig. 5 (A) Excised recurrent solid tumors from different treatment groups on the 30th day. (B) Tumor weight statistics chart ($n = 5$). (C) γ-H2AX analysis of excised recurrent tumor on the 30th day. (D) TUNEL analysis of excised recurrent tumor on the 30th day. Scale bar = 50 μm. (E) Mean fluorescence intensity of γ-H2AX ($n = 5$). (F) Mean fluorescence intensity of TUNEL ($n = 5$).

situations of unfeasible complete tumor removal is common, especially in advanced-stage cancers. Upon treating the tumor recurrence model with the composite cryogel loaded with cisplatin–CS–calcium alginate MPs, the following observations were mad. As depicted in Fig. 5A and B. First, recurrent tumors in the cryogel group (0.57 ± 0.23 g) exhibited rapid growth, with no statistically significant difference in inhibiting recurrent tumors observed in cryogel-M-1 (0.49 ± 0.06 g) compared with the cryogel group. Notably, a statistically significant reduction occurred in the volume of recurrent tumors in cryogel-M-2 (0.27 ± 0.10 g) compared with cryogel-M-1 and the cryogel group. A further significant decrease in recurrent tumor volume was observed in cryogel-M-3 (0.13 ± 0.05 g) compared with the cryogel group and cryogel-M-1. Cryogel-M-4 (0.06 ± 0.01 g) exhibited the most substantial reduction in recurrent tumor volume compared with cryogel-M-3, cryogel-M-2, cryogel-M-1, and the cryogel group, with a statistically significant difference.

In summary, *in vivo* tumor recurrence transplantation experiments demonstrated that as the concentration of MPs in the cryogel increased, the volume of recurrent tumors decreased. Tumor-weight data corroborated this trend, showing that higher MP concentrations in the composite loaded with cisplatin–CS–calcium alginate MPs led to smaller recurrent tumor weights in mice.

To further investigate the mechanism of action of MP-rich cryogel to inhibit tumor recurrence and metastasis, immunofluorescence was performed on frozen sections of recurrent tumors. As depicted in Fig. 5C, blue fluorescence labeling is the cell nucleus, and green fluorescence labeling is γ-H2AX protein expression. Immunofluorescence assay in Fig. 5E results showed that γ-H2AX was a DNA double-strand break marker, and the cryogel group did not have γ-H2AX expression. Meanwhile, cryogel-M-1, cryogel-M-2, cryogel-M-3, and cryogel-M-4 showed γ-H2AX expression. γ-H2AX expression increased with increased concentration of MPs in cryogel. This finding further verified the conclusion drawn from the *in vitro* experiments that cryogel loaded with MPs can slow release cisplatin and play the roles of tumor killing and proliferation inhibition. Thus, it was an ideal material for filling and preventing tumor recurrence.

Cisplatin, a platinum-based chemotherapeutic agent, shows promise in the treatment of breast cancer. Understanding the mechanisms underlying its cytotoxic effects, particularly through apoptosis induction, is crucial for optimizing its clinical application.[43] Cisplatin induces apoptosis, a programmed-cell-death process in MDA-MB-231 breast cancer cells.[44] According to previous studies, apoptosis is one of the reasons why cisplatin acts on cells to cause their death.[44] To further understand the tumor apoptosis, we used the terminal deoxynucleotidyl transferase dUTP nick-end labeling (TUNEL) assay. It is a widely used method in molecular biology and pathology for detecting apoptotic cells within a tissue or cell culture sample. The assay relies on the principle of labeling exposed 3′-OH ends of DNA fragments generated during apoptosis. Fig. 5D and F illustrates the results of the TUNEL analysis, wherein green fluorescence represents FITC-labeled TUNEL, and blue fluorescence represents cell nuclei. No TUNEL expression was observed in the cryogel group. Conversely, TUNEL expression was evident in cryogel-M-1, cryogel-M-2, cryogel-M-3, and cryogel-M-4, with the extent of TUNEL expression directly correlating with the concentration of MPs within the cryogel. The rise in TUNEL expression was proportional to the increase in MP concentration within the cryogel. The presence of TUNEL-positive cells in the cryogel-M groups indicated an increase in the number of apoptotic tumor cells with increased concentration of MPs in the composite cryogel loaded with cisplatin–CS–calcium alginate MPs. This observation provided further evidence that cisplatin released from the cryogel exerted an inhibitory effect on cell replication by acting on DNA, ultimately leading to apoptosis.

Overall, our results suggested that the hydrogel platform can be used to prevent breast tumor recurrence after surgery. *In vivo* anti-recurrence experiments demonstrated a novel strategy as a potential breast reconstruction material, the hydrogel platform should be a favorable filler for dissected empty space after surgery, and had the potential to support the attachment of normal breast cells and adipose cells for the following tissue repair.

4. Conclusion

We developed hydrogel loaded with cisplatin–CS–calcium alginate MPs. By investigating the differences in microstructure and mechanical properties of the gel material loaded with MPs at various concentrations, we demonstrated that this composite gel material had a porous structure and mechanical strength. It can be tailored to achieve the desired mechanical performance by adjusting the concentration of the loaded MPs. We further examined the impact of gel materials loaded with MPs at different concentrations on *in vitro* coagulation and *in vivo* hemostatic effects. Results indicated that this composite material can effectively substitute commercial gelatin sponges, efficiently treating oozing hemorrhage through its porous structure, blood absorption capabilities, and enhanced coagulation effects attributed to the CS and gelatin components. Accordingly, effective hemostasis ensured. Lastly, we investigated the differences in the antitumor effects of gel materials loaded with MPs at varying concentrations *in vitro* and *in vivo*. The findings revealed that as the concentration of loaded MPs increased, the antitumor efficacy also increased.

Therefore, this composite material can provide effective chemotherapy post-breast cancer surgery while reducing the risk of tumor recurrence and metastasis by absorbing circulating tumor cells from postoperative residues or bleeding. This study also highlights the potential of this composite material in breast reconstruction, offering a dual benefit of tumor safety and aesthetic outcomes in postoperative implants.

Ethical statement

All animal procedures were performed in accordance with the Regulations for the Administration of Affairs Concerning Experimental Animals of Southern Medical University (P. R. China) and approved by the Southern Medical University Animal Ethics Committee (SYXK(粤)2016-0167).

Conflicts of interest

The authors declare no conflict of interest.

References

1 F. Bray, J. Ferlay, I. Soerjomataram, R. L. Siegel, L. A. Torre and A. Jemal, *Ca-Cancer J. Clin.*, 2018, **68**, 394–424.
2 R. L. Siegel, K. D. Miller and A. Jemal, *Ca-Cancer J. Clin.*, 2019, **69**, 7–34.
3 R. L. Siegel, K. D. Miller and A. Jemal, *Ca-Cancer J. Clin.*, 2020, **70**, 7–30.
4 S. Y. Hwang, S. Park and Y. Kwon, *Pharmacol. Ther.*, 2019, **199**, 30–57.
5 L. Moore-Smith, A. Forero-Torres and E. Stringer-Reasor, *Surg. Clin. North Am.*, 2018, **98**, 773–785.
6 E. Botteri, V. Bagnardi, N. Rotmensz, O. Gentilini, D. Disalvatore, B. Bazolli, A. Luini and U. Veronesi, *Ann. Oncol.*, 2010, **21**, 723–728.
7 A. Fabisiewicz, M. Szostakowska-Rodzos, A. J. Zaczek and E. A. Grzybowska, *Int. J. Mol. Sci.*, 2020, **21**(5), 1671.
8 S. Wang, F. Sun, H. Huang, K. Chen, Q. J. Li, L. Zhang, E. Wang, C. Wang, H. Zhang, A. Q. Yuan, B. Chen, T. Deng, Y. Liu, J. Sun, D. Liu, Y. Yu, Y. Fang, N. Jiang, D. Wu, H. Fang, Y. Bai, S. Xing, Y. Ni, Q. Fan, A. Yu, C. Sun, Y. Tang, N. Li, B. Xu and J. He, *Cancer Cell*, 2021, **39**, 7–8.
9 X. Yang, L. Gao, Y. Wei, B. Tan, Y. Wu, C. Yi and J. Liao, *J. Nanobiotechnol.*, 2021, **19**, 307.
10 T. J. Puls, C. S. Fisher, A. Cox, J. M. Plantenga, E. L. McBride, J. L. Anderson, C. J. Goergen, M. Bible, T. Moller and S. L. Voytik-Harbin, *Sci. Rep.*, 2021, **11**, 2711.
11 K. Lerdchai, J. Kitsongsermthon, J. Ratanavaraporn, S. Kanokpanont and S. Damrongsakkul, *J. Pharm. Sci.*, 2016, **105**, 221–230.
12 G. J. Dugbartey, L. J. Peppone and I. A. de Graaf, *Toxicology*, 2016, **371**, 58–66.
13 P. S. Ooi, N. Draman, R. Muhamad, S. S. M. Yusoff, N. M. Noor, J. Haron and I. S. A. Hadi, *Sex. Med.*, 2021, **9**, 100351.
14 X. Li, F. Xu, Y. He, Y. Li, J. Hou, G. Yang and S. Zhou, *Adv. Funct. Mater.*, 2020, **30**, 2004851.
15 X. Sun, Q. Lang, H. Zhang, L. Cheng, Y. Zhang, G. Pan, X. Zhao, H. Yang, Y. Zhang, H. A. Santos and W. Cui, *Adv. Funct. Mater.*, 2017, **27**, 1604617.
16 Y. Wu, H. Wang, F. Gao, Z. Xu, F. Dai and W. Liu, *Adv. Funct. Mater.*, 2018, **28**, 1801000.
17 X. Yang, C. Hu, F. Tong, R. Liu, Y. Zhou, L. Qin, L. Ouyang and H. Gao, *Adv. Funct. Mater.*, 2019, **29**, 1901896.
18 P. N. Navya, A. Kaphle, S. P. Srinivas, S. K. Bhargava, V. M. Rotello and H. K. Daima, *Nano Convergence*, 2019, **6**, 23.
19 A. Partovinia and E. Vatankhah, *Carbohydr. Polym.*, 2019, **209**, 389–399.
20 J. T. Kaifi, M. Kunkel, A. Das, R. A. Harouaka, D. T. Dicker, G. Li, J. Zhu, G. A. Clawson, Z. Yang, M. F. Reed, N. J. Gusani, E. T. Kimchi, K. F. Staveley-O'Carroll, S. Y. Zheng and W. S. El-Deiry, *Cancer Biol. Ther.*, 2015, **16**, 699–708.
21 X. Zhao, B. Guo, H. Wu, Y. Liang and P. X. Ma, *Nat. Commun.*, 2018, **9**(1), 2784.
22 M. Sepantafar, R. Maheronnaghsh, H. Mohammadi, F. Radmanesh, M. M. Hasani-Sadrabadi, M. Ebrahimi and H. Baharvand, *Trends Biotechnol.*, 2017, **35**, 1074–1087.
23 A. Borchers and T. Pieler, *Genes*, 2010, **1**, 413–426.
24 C. Jaiswal, T. Gupta, P. K. Jadi, J. C. Moses and B. B. Mandal, *Biomater. Adv.*, 2023, **145**, 213224.
25 J. Zhang, C. Chen, A. Li, W. Jing, P. Sun, X. Huang, Y. Liu, S. Zhang, W. Du, R. Zhang, Y. Liu, A. Gong, J. Wu and X. Jiang, *Nat. Nanotechnol.*, 2021, **16**, 538–548.
26 K. Meng, C. Yao, Q. Ma, Z. Xue, Y. Du, W. Liu and D. Yang, *Adv. Sci.*, 2019, **6**, 1802112.
27 J. Van Hoorick, P. Gruber, M. Markovic, M. Tromayer, J. Van Erps, H. Thienpont, R. Liska, A. Ovsianikov, P. Dubruel and S. Van Vlierberghe, *Biomacromolecules*, 2017, **18**, 3260–3272.
28 A. M. Florea and D. Busselberg, *Cancers*, 2011, **3**, 1351–1371.
29 M. S. Cohen, S. Cai, Y. Xie and M. L. Forrest, *Am. J. Surg.*, 2009, **198**, 781–786.
30 A. Wilmes, C. Bielow, C. Ranninger, P. Bellwon, L. Aschauer, A. Limonciel, H. Chassaigne, T. Kristl, S. Aiche, C. G. Huber, C. Guillou, P. Hewitt, M. O. Leonard, W. Dekant, F. Bois and P. Jennings, *Toxicol. In Vitro*, 2015, **30**, 117–127.
31 R. Li, Y. Zhang, Z. Lin, Q. Lei, Y. Liu, X. Li, M. Liu, G. Wu, S. Luo, H. Wang, X. Zheng, L. Li, N. Ao and Z. Zha, *Composites, Part B*, 2021, **221**, 109031.
32 Z. Dong, L. Feng, Y. Chao, Y. Hao, M. Chen, F. Gong, X. Han, R. Zhang, L. Cheng and Z. Liu, *Nano Lett.*, 2019, **19**, 805–815.
33 J. Chen, D. Huang, L. Wang and J. Hou, *J. Colloid Interface Sci.*, 2020, **574**, 162–173.
34 A. D. Arya, P. M. Hallur, A. G. Karkisaval, A. Gudipati, S. Rajendiran, V. Dhavale, B. Ramachandran, A. Jayaprakash, N. Gundiah and A. Chaubey, *ACS Appl. Mater. Interfaces*, 2016, **8**, 22005–22017.
35 Z. Zhang, G. Kuang, S. Zong, S. Liu, H. Xiao, X. Chen, D. Zhou and Y. Huang, *Adv. Mater.*, 2018, **30**, e1803217.
36 H. Kaur, N. Mishra, B. Khurana, S. Kaur and D. Arora, *Curr. Mol. Pharmacol.*, 2021, **14**(3), 381–398.
37 M. M. Alsmadi, R. M. Obaidat, M. Alnaief, B. A. Albiss and N. Hailat, *AAPS PharmSciTech*, 2020, **21**(5), 191.
38 K. Li, H. Yan, W. Guo, M. Tang, X. Zhao, A. Tong, Y. Peng, Q. Li and Z. Yuan, *Exp. Cell Res.*, 2018, **366**, 24–33.
39 H. Zhu, H. Luo, W. Zhang, Z. Shen, X. Hu and X. Zhu, *Drug Des., Dev. Ther.*, 2016, **10**, 1885–1895.
40 Z. Gao, M. Shi, Y. Wang, J. Chen and Y. Ou, *Pathol., Res. Pract.*, 2019, **215**, 152422.
41 H. S. Oberoi, N. V. Nukolova, A. V. Kabanov and T. K. Bronich, *Adv. Drug Delivery Rev.*, 2013, **65**, 1667–1685.
42 X. Duan, C. He, S. J. Kron and W. Lin, *Wiley Interdiscip. Rev.: Nanomed. Nanobiotechnol.*, 2016, **8**, 776–791.
43 Z. H. Siddik, *Oncogene*, 2003, **22**, 7265–7279.
44 N. Bhagya, A. Prabhu, P. D. Rekha and K. R. Chandrashekar, *Synergy*, 2020, **10**, 100063.